Journal of Petroleum Science and Engineering 217 (2022) 110935

Contents lists available at ScienceDirect

Journal of Petroleum Science and Engineering

journal homepage: www.elsevier.com/locate/petrol

Robertson-Stiff rheological model in fracture flow

Alexandre Lavrov

Norwegian University of Science and Technology, Trondheim, Norway

ARTICLE INFO

Keywords:
Robertson-stiff model
Fluid
Flow
Fracture

ABSTRACT

Robertson-Stiff rheological model has been recently shown to provide a more accurate description of a drilling fluid than the Herschel-Bulkley model. In this short communication, a relation between the pressure gradient and the average fluid velocity in a fracture is derived for the Robertson-Stiff model. Practical use of the model is demonstrated using an example of one-dimensional radial flow with a Robertson-Stiff fluid displacing a Newtonian fluid in a horizontal fracture.

1. Introduction

Lost circulation has been a known drilling problem for decades (Onyia, 1994). This problem becomes steadily more common and more expensive as the drilling depth increases and the mud weight window becomes narrow, e.g. in deepwater drilling and infill drilling (Lavrov, 2016). Theoretical studies of mud losses are often based on numerical modelling of drilling fluid invasion in natural fractures (Lavrov, 2005). In such models, the drilling fluid is represented as a generalized Newtonian fluid with a yield stress. Typically, Bingham or Herschel-Bulkley rheology is assumed for drilling fluids (Caenn et al., 2011; Majidi et al., 2008, 2010a; Rodríguez de Castro and Radilla, 2017). The validity of Herschel-Bulkley rheology for drilling fluids was recently reviewed in (Cayeux, 2020). It was found that the results of rheometric measurements on drilling fluid samples can be fitted with the Herschel-Bulkley model at low shear rates. A better fit to the experimental data in the entire range of shear rates can, according to (Cayeux, 2020), be obtained by using the Robertson-Stiff rheological model (Robertson and Stiff, 1976).

In a simple shear flow, the relationship between shear stress and strain rate in the Robertson-Stiff model is expressed by

$$\tau = A(|\dot{\gamma}| + C)^B \tag{1}$$

where τ is the shear stress; $\dot{\gamma}$ is the shear rate; A, B, C are fitting parameters. From Eq. (1), the yield stress is equal to AC^B. Thus, Eq. (1) can be re-written as follows:

$$\tau = \tau_Y \left(\frac{|\dot{\gamma}|}{C} + 1\right)^B \tag{2}$$

where τ_Y is the yield stress. When $\tau < \tau_Y$, the shear rate is zero, $\dot{\gamma} = 0$.

In a general type of flow of a generalized Newtonian flow, the shear stress tensor, $\mathbf{S}$, is related to the shear rate tensor, $\mathbf{D}$, as follows (Irgens, 2008):

$$\mathbf{S} = 2\mu_a(\Gamma)\mathbf{D} \tag{3}$$

where $\Gamma = \sqrt{2\mathbf{D} : \mathbf{D}}$ is a shear rate measure; μ_a is the apparent viscosity, for the Robertson-Stiff model given by:

$$\mu_a = \frac{\tau_Y}{\Gamma}\left(\frac{\Gamma}{C} + 1\right)^B \tag{4}$$

For comparison, the apparent viscosity for a Herschel-Bulkley fluid is given by:

$$\mu_a = K\Gamma^{n-1} + \frac{\tau_Y}{\Gamma} \tag{5}$$

where K is consistency index; n is the flow index; τ_Y is the yield stress. In a simple shear flow, the shear stress *vs* shear rate relationship for a Herschel-Bulkley fluid is given by:

$$\tau = \tau_Y + K|\dot{\gamma}|^n \tag{6}$$

To illustrate the Robertson-Stiff and Herschel-Bulkley models, the shear stress *vs* shear rate curves for both are shown in Fig. 1. The following rheological properties were used in Fig. 1: Herschel-Bulkley fluid: $\tau_Y = 10$ Pa, $n = 0.8$, $K = 0.01$ Pa $s^{0.8}$; Robertson-Stiff fluid: $\tau_Y = 10$ Pa, $B = n = 0.8$, $C = (\tau_Y/K)^{1/n} = 5623$ s^{-1}. It is evident from Fig. 1 that, with the above choice of rheological properties, the Herschel-Bulkley model has a slightly larger apparent viscosity than the Robertson-Stiff fluid. This is as expected since, for $0 < n < 1$, $(|a| + |b|)^{1/n} \leq |a|^{1/n} + |b|^{1/n}$.

E-mail address: alexandre.lavrov@ntnu.no.

https://doi.org/10.1016/j.petrol.2022.110935
Received 11 March 2022; Received in revised form 17 June 2022; Accepted 30 July 2022
Available online 3 August 2022
0920-4105/© 2022 The Author. Published by Elsevier B.V. This is an open access article under the CC BY license (http://creativecommons.org/licenses/by/4.0/).

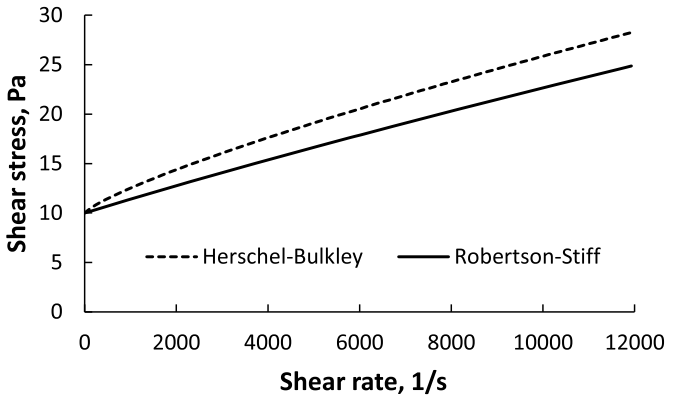

Fig. 1. *Flow curves for a Herschel-Bulkley fluid with* $\tau_Y = 10$ Pa, $n = 0.8$, $K = 0.01$ Pa $s^{0.8}$ *and a Robertson-Stiff fluid with* $\tau_Y = 10$ Pa, $B = n = 0.8$, $C = (\tau_Y/K)^{1/n} = 5623\ s^{-1}$.

When computing fluid flow in a rock fracture, a relationship between the pressure gradient and the flow rate (or fluid velocity averaged across the fracture aperture) is used. Such a relationship is usually derived assuming that the lubrication theory approximation is valid (Zimmerman et al., 1991). In particular, the flow is Stokes flow (Re → 0), and fracture faces are sufficiently smooth. Under these assumptions, the *average* fluid velocity of e.g. a Herschel-Bulkley fluid in a fracture of aperture w is given by (Morris et al., 2015):

$$\mathbf{v}=\begin{cases} 0 \text{ if } |\nabla P|<\dfrac{2\tau_Y}{w} \\ \dfrac{2n}{n+1}\dfrac{\nabla P}{K^{1/n}w|\nabla P|^2}\left[\dfrac{n}{2n+1}\dfrac{1}{|\nabla P|}\left(\dfrac{w|\nabla P|}{2}-\tau_Y\right)^{(2n+1)/n}-\dfrac{w}{2}\left(\dfrac{w|\nabla P|}{2}-\tau_Y\right)^{(n+1)/n}\right] \text{ if } |\nabla P|>\dfrac{2\tau_Y}{w} \end{cases} \tag{7}$$

where ∇P is the pressure gradient in the plane of the fracture defined by Cartesian coordinates x_1, x_2. The third coordinate axis, x_3, is directed normal to the fracture plane; $x_3 = 0$ defines the center plane between the fracture faces. It should be noted that $\mathbf{v}$ is understood as the velocity averaged across the fracture aperture, i.e. it is the flow rate divided by the fracture aperture, w.

The objectives of this study are (i) to derive a relationship between the average fluid velocity, $\mathbf{v}$, and the pressure gradient, ∇P, in fracture flow for the Robertson-Stiff model [similar to Eq. (7) for Herschel-Bulkley fluid], and (ii) to demonstrate practical use of this relationship in a 1D simulation of fluid flow and displacement from a borehole into a horizontal fracture.

It should be noted that an attempt to derive a relationship between the average fluid velocity and the pressure gradient in fracture flow for the Robertson-Stiff model was made already in the original paper by Robertson and Stiff. Unfortunately, a mistake was made in their derivation: The authors did not recognize the existence of the unyielded zone around the fracture's mid-plane. Consequently, the published results are incorrect (more exactly, they are correct only in the asymptotic case of $|\nabla P| \to \infty$). The present contribution aims to rectify this issue.

2. Lubrication flow with Robertson-Stiff rheological model

Assuming the lubrication theory approximation conventionally used in fracture flow modelling (Zimmerman et al., 1991), the flow is laminar, the fluid velocity normal to the fracture plane is zero, and the strain rate tensor is thus given by:

$$\mathbf{D}=\frac{1}{2}\begin{bmatrix} 0 & 0 & \dfrac{\partial u_1}{\partial x_3} \\ 0 & 0 & \dfrac{\partial u_2}{\partial x_3} \\ \dfrac{\partial u_1}{\partial x_3} & \dfrac{\partial u_2}{\partial x_3} & 0 \end{bmatrix} \tag{8}$$

where u_1 and u_2 are the in-plane components of the fluid velocity.

The stress tensor is given by

$$\mathbf{S}=\begin{bmatrix} 0 & 0 & \tau_{13} \\ 0 & 0 & \tau_{23} \\ \tau_{13} & \tau_{23} & 0 \end{bmatrix} \tag{9}$$

Combining Eqs. (8) and (9) with Eqs. (3) and (4) yields:

$$\left.\begin{matrix}\tau_{13}\\ \tau_{23}\end{matrix}\right\} = \tau_Y \frac{\left\{\frac{1}{C}\left[\left(\frac{\partial u_1}{\partial x_3}\right)^2+\left(\frac{\partial u_2}{\partial x_3}\right)^2\right]^{1/2}+1\right\}^B}{\left[\left(\frac{\partial u_1}{\partial x_3}\right)^2+\left(\frac{\partial u_2}{\partial x_3}\right)^2\right]^{1/2}} \cdot \left\{\begin{matrix}\dfrac{\partial u_1}{\partial x_3}\\ \dfrac{\partial u_2}{\partial x_3}\end{matrix}\right. \tag{10}$$

Momentum conservation under the assumptions of the lubrication theory approximation reduces to the following two equations (Majidi et al., 2010a; Morris et al., 2015):

$$\left.\begin{matrix}\tau_{13}\\ \tau_{23}\end{matrix}\right\} = x_3 \cdot \left\{\begin{matrix}\dfrac{\partial P}{\partial x_1}\\ \dfrac{\partial P}{\partial x_2}\end{matrix}\right. \tag{11}$$

After some algebra, Eqs. (10) and (11) yield:

$$\left.\begin{matrix}\dfrac{\partial u_1}{\partial x_3}\\ \dfrac{\partial u_2}{\partial x_3}\end{matrix}\right\} = -\frac{C}{|\nabla P|}\left[\left(-\frac{x_3|\nabla P|}{\tau_Y}\right)^{1/B}-1\right] \cdot \left\{\begin{matrix}\dfrac{\partial P}{\partial x_1}\\ \dfrac{\partial P}{\partial x_2}\end{matrix}\right. \tag{12}$$

When a yield-stress fluid flows in a fracture, a plug of unyielded material is formed around the center plane of the fracture (i.e. around $x_3 = 0$) where $(\tau_{13}^2+\tau_{23}^2)^{1/2} < \tau_Y$. The thickness of the unyielded plug is given by $2\tau_Y/|\nabla P|$. Thus, in order to have flow, the pressure gradient must be greater than $2\tau_Y/w$.

Integrating Eq. (12) over half of the fracture aperture ($x_3 < 0$) and using the no-slip boundary condition at the fracture wall, i.e. $u_1 = u_2 =$

0 at $x_3 = -w/2$, yields the following velocity profile outside the unyielded plug region, $-w/2 < x_3 < -\tau_Y/|\nabla P|$:

$$\left.\begin{matrix} u_1 \\ u_2 \end{matrix}\right\} = \frac{C}{|\nabla P|}\left[\frac{w}{2} - \frac{B}{B+1}\frac{\tau_Y}{|\nabla P|}\left(\frac{w|\nabla P|}{2\tau_Y}\right)^{(B+1)/B} + x_3 + \frac{B}{B+1}\frac{\tau_Y}{|\nabla P|}\left(-\frac{x_3|\nabla P|}{\tau_Y}\right)^{(B+1)/B}\right]\cdot\left\{\begin{matrix} \frac{\partial P}{\partial x_1} \\ \frac{\partial P}{\partial x_2} \end{matrix}\right. \tag{13}$$

Within the unyielded plug, the velocity is constant and can be obtained from Eq. (13) by substituting $x_3 = -\tau_Y/|\nabla P|$. Thus, at $-\tau_Y/|\nabla P| < x_3 < 0$, the fluid velocity is equal to (subscript "p" stands for "plug"):

$$\left.\begin{matrix} u_{p1} \\ u_{p2} \end{matrix}\right\} = \frac{C}{|\nabla P|}\left[\frac{w}{2} - \frac{B}{B+1}\frac{\tau_Y}{|\nabla P|}\left(\frac{w|\nabla P|}{2\tau_Y}\right)^{(B+1)/B} - \frac{\tau_Y}{(B+1)|\nabla P|}\right]\cdot\left\{\begin{matrix} \frac{\partial P}{\partial x_1} \\ \frac{\partial P}{\partial x_2} \end{matrix}\right. \tag{14}$$

Flow rate is obtained by integrating the velocity from $x_3 = -w/2$ to $x_3 = 0$ and multiplying the result by two. Dividing the result by w yields the following average velocity for fracture flow of a Robertson-Stiff fluid:

$$\mathbf{v} = \begin{cases} 0 \quad \text{if } |\nabla P| < \dfrac{2\tau_Y}{w} \\ \left[\dfrac{Cw}{4|\nabla P|} - \dfrac{C\tau_Y^2}{(2B+1)w|\nabla P|^3} - \dfrac{BC\tau_Y}{(2B+1)|\nabla P|^2}\left(\dfrac{w|\nabla P|}{2\tau_Y}\right)^{(B+1)/B}\right]\nabla P \quad \text{if } |\nabla P| > \dfrac{2\tau_Y}{w} \end{cases} \tag{15}$$

If the flow is along one of the in-plane coordinate axes, e.g. x_1, the average velocity is given by:

$$v_1 = \begin{cases} 0 \quad \text{if } \left|\dfrac{\partial P}{\partial x_1}\right| < \dfrac{2\tau_Y}{w} \\ \left[\dfrac{Cw}{4|\partial P/\partial x_1|} - \dfrac{C\tau_Y^2}{(2B+1)w|\partial P/\partial x_1|^3} - \dfrac{BC\tau_Y}{(2B+1)|\partial P/\partial x_1|^2}\left(\dfrac{w|\partial P/\partial x_1|}{2\tau_Y}\right)^{(B+1)/B}\right]\dfrac{\partial P}{\partial x_1} \quad \text{if } \left|\dfrac{\partial P}{\partial x_1}\right| > \dfrac{2\tau_Y}{w} \end{cases} \tag{16}$$

As an example of fluid velocity *vs* pressure gradient for a fracture with $w = 1$ mm is shown in Fig. 2. The fluid properties are the same as those in Fig. 1. Since the Herschel-Bulkley fluid has a higher apparent viscosity than its Robertson-Stiff counterpart (Fig. 1), the dashed line in Fig. 2 runs lower than the solid line.

3. Application example: one-dimensional radial flow and displacement in a horizontal fracture

As an example application of the Robertson-Stiff fluid flow in a fracture, we consider a radial, one-dimensional problem in which a yield-stress fluid displaces a Newtonian fluid. A horizontal infinite fracture is penetrated by a borehole, and a radial flow of drilling mud from the borehole into the fracture ensues.

Theoretical models of mudlosses often assume that only one fluid is flowing in the fracture, namely the yield-stress fluid invading the fracture (Majidi et al., 2008, 2010a). This assumption might be valid when the formation fluid is a gas. The validity of this assumption in the case when the formation fluid is water or oil is less obvious. An example of a more realistic work where two fluids were properly considered is (Majidi et al., 2010b). Following the same path, we assume that, prior to drilling, the fracture was filled with a Newtonian fluid of viscosity μ. This fluid is called "fluid in place", or "fluid 1" below. The invading fluid is a yield-stress fluid described by the Robertson-Stiff model and is called "invading fluid" or "fluid 2". We assume laminar incompressible flow. We further assume that the overbalance pressure remains constant during the simulation since our goal here is simply to demonstrate the application of the model rather than to study a realistic operational scenario where the borehole pressure, P_w, would be varying over time.

The fracture is circular in plane; the borehole meets the fracture in the center of the fracture. The external radius of the fracture is R_{ext} (the "reservoir radius"). Constant fluid pressure P_0 is assumed at the external boundary; the initial formation pressure is equal to P_0. The radius of the borehole is R_w.

Mass balance equation for radial flow is given by

$$\frac{\partial}{\partial r}(rv) = 0 \tag{17}$$

where r is the radial coordinate; u is the (radial) average fluid velocity. Solution to Eq. (17) is given by

$$v = \frac{C_v}{r} \tag{18}$$

where C_v is an integration constant. In order to find C_v, we assume that pressure is continuous across the interface between the invading fluid and the fluid in place, i.e. the interfacial tension pressure is equal to zero.

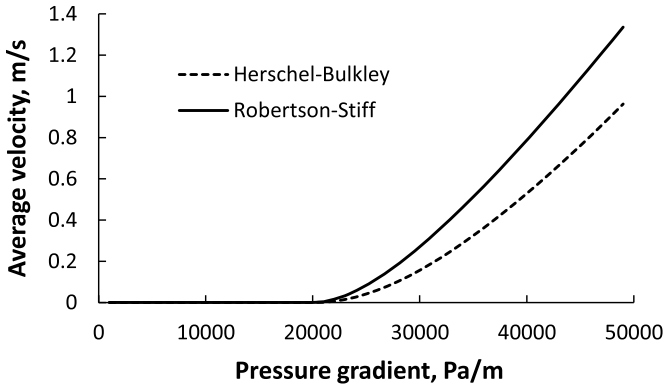

Fig. 2. Average fluid velocity in a fracture of aperture w = 1 mm vs pressure gradient. The fluid properties are given in the caption to Fig. 1.

Denote the radial position of the interface $\widetilde{R}$ and the pressure at the interface $\widetilde{P}$. Then, at $r > \widetilde{R}$, the fracture is filled with the Newtonian formation fluid, and the averaged fluid velocity is given by the cubic law:

$$v = \frac{w^2}{12\mu}\frac{\widetilde{P} - P_0}{r\log(R_{ext}/\widetilde{R})} \quad \text{at} \quad r > \widetilde{R} \tag{19}$$

Combining Eqs. (18) and (19) yields:

$$C_v = \frac{w^2}{12\mu}\frac{\widetilde{P} - P_0}{\log(R_{ext}/\widetilde{R})} \tag{20}$$

The interface pressure can be obtained by integrating the pressure gradient from $r = R_w$ to $r = \widetilde{R}$:

$$\widetilde{P} = P_w + \int_{R_w}^{\widetilde{R}} \frac{\partial P}{\partial r}\mathrm{d}r \tag{21}$$

The advancement of the interface is given by an ordinary differential equation stating that the interface advances with the velocity equal to the averaged fluid velocity at the interface (since the fracture has porosity equal to 1):

$$\frac{d\widetilde{R}}{dt} = \frac{w^2}{12\mu}\frac{\widetilde{P} - P_0}{\widetilde{R}\log(R_{ext}/\widetilde{R})} \tag{22}$$

Initial condition for the pressure is given by:

$$P = P_0 \quad \text{at} \quad R_w < r < R_{ext}, t = 0 \tag{23}$$

Initial condition for the interface position is given by:

$$\widetilde{R} = R_w + \varepsilon\Delta r_0 \quad \text{at} \quad t = 0 \tag{24}$$

where ε is a small number (10^{-4}); Δr_0 is the distance between the two grid nodes closest to the borehole wall (the node on the wall, at $r = R_w$, and the next node, at $r = R_w + \Delta r_0$). Setting the initial interface position exactly at the borehole wall, i.e. $\widetilde{R} = R_w$, would cause a numerical error since the interface must be located between two grid nodes in order to be identified.

Boundary conditions are given by:

$$P = P_0 \quad \text{at} \quad r = R_{ext} \tag{25}$$

$$P = P_w \quad \text{at} \quad r = R_w \tag{26}$$

The above equations are solved numerically at each timestep as follows:

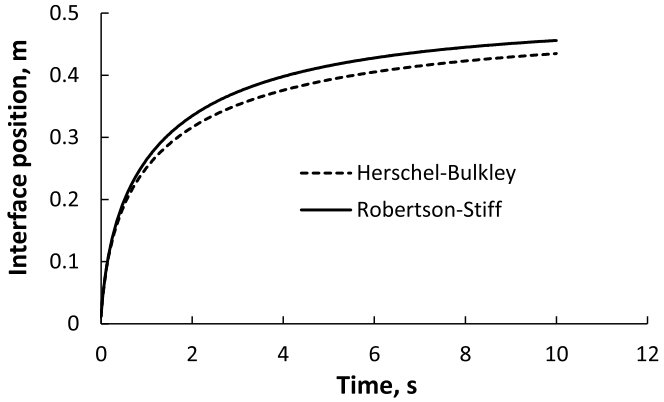

Fig. 3. Position of fluid interface between the invading yield-stress drilling fluid and the Newtonian formation fluid (water) vs time. Fracture aperture: w = 1 mm. Overbalance 10^4 Pa. Fluid properties are given in the caption to Fig. 1.

1) The velocity integration constant, C_v, is found by solving Eqs. (20) and (21) simultaneously, by using the bisection method. The pressure gradient for yield-stress fluid in Eq. (21) is found from Eq. (16) by Newton's method; Eq. (21) is integrated numerically by trapezoïdal rule.
2) Velocity is updated at each node and at $r = \widetilde{R}$ by using Eq. (18).
3) The position of the interface, $\widetilde{R}$, is updated by the predictor-corrector (Heun's) method. It was shown earlier that predictor-corrector provides a reasonable trade-off between accuracy and computational cost in one-dimensional flows where a yield-stress fluid displaces a Newtonian fluid (Lavrov, 2021).

Logarithmic grid is used, with progressive refinement towards the borehole wall.

It should be noted that our solution procedure is slightly different from the one used in (Majidi et al., 2010b). Namely, an infinite fracture was assumed in (Majidi et al., 2010b), with the solution for fluid 1 given by an integral. Fluid 1 was assumed compressible (Majidi et al., 2010b).

An example of the calculation is given in Fig. 3, alongside with a similar calculation for a Herschel-Bulkley fluid. The following input data were used: fracture aperture $w = 1$ mm; overbalance 1 kPa; $R_{ext} = 100$ m; $R_w = 0.1$ m. Viscosity of the formation fluid was μ = 0.001 Pa s (water). Properties of the invading fluid are given in the caption to Fig. 1. Since the Herschel-Bulkley fluid has a higher apparent viscosity than its Robertson-Stiff counterpart (Fig. 1), the dashed line in Fig. 3 is running below the solid line, i.e. the advancement of the interface is slower for the former.

4. Discussion

The Robertson-Stiff model is one of the few non-Newtonian rheological models that admit analytical, closed-form solution for the flow rate as a function of the pressure gradient in fracture flow. Other such models are Herschel-Bulkley, power-law, and Bingham models. A closed-form solution speeds up computations where it is used as a closure law, e.g. in hydraulic fracturing simulations or in a mud loss model like the one used in Section 3. Using rheological models for which a closed-form solution is not available is still possible but entails extra compute time or requires approximating the rheological model, e.g. as was suggested in (Wrobel, 2020). The closed-form solution derived for the Robertson-Stiff model in this article makes a useful contribution to the bank of available non-Newtonian fluid models that can be employed in fracture flow simulations. One such application is provided by the demonstration example in Section 3.

It should be noted that the application example provided in Section 3 is intended for demonstration purposes only. It is not an advanced fluid

loss model. A number of additional factors should be considered when constructing more advanced models of that sort, e.g. arbitrary fracture inclination (with the resulting gravity effects), fracture compressibility, and fracture roughness.

5. Conclusion

Relation between the pressure gradient and the average fluid velocity has been derived for the Robertson-Stiff rheological model for both one-dimensional and two-dimensional fracture flow. An example application for 1D radial flow with a Robertson-Stiff fluid displacing a Newtonian fluid in a horizontal fracture has been presented.

Creit author statement

A. Lavrov: Conceptualization; Formal analysis; Investigation; Methodology; Software; Visualization; Writing – original draft; Writing – review & editing.

Declaration of competing interest

The authors declare that they have no known competing financial interests or personal relationships that could have appeared to influence the work reported in this paper.

References

Caenn, R., Darley, H.C.H., Gray, G.R., 2011. Composition and Properties of Drilling and Completion Fluids. Elsevier, Amsterdam.

Cayeux, E., 2020. Time, pressure and temperature dependent rheological properties of drilling fluids and their automatic measurements. In: SPE Paper 199641 Presented at the IADC/SPE International Drilling Conference and Exhibition.

Irgens, F., 2008. Continuum Mechanics. Springer, p. 661.

Lavrov, A., 2005. Modeling flow of a biviscous fluid from borehole into rock fracture. ASME Journal of Applied Mechanics 73 (1), 171–173.

Lavrov, A., 2016. Lost Circulation: Mechanisms and Solutions. Elsevier, Oxford, p. 264.

Lavrov, A., 2021. Fluid displacement in a 2D DFN fracture: time integration of the interface position. Transport Porous Media 139 (2), 247–269.

Majidi, R., Miska, S.Z., Ahmed, R., Yu, M., Thompson, L.G., 2010a. Radial flow of yield-power-law fluids: numerical analysis, experimental study and the application for drilling fluid losses in fractured formations. J. Petrol. Sci. Eng. 70 (3), 334–343.

Majidi, R., Miska, S.Z., Thompson, L.G., Yu, M., 2008. Quantitative analysis of mud losses in naturally fractured reservoirs: the effect of rheology. In: SPE Paper 114130 Presented at the SPE Western Regional and Pacific Section AAPG Joint Meeting.

Majidi, R., Miska, S.Z.Z., Yu, M., Thompson, L.G.G., Zhang, J., 2010b. Quantitative analysis of mud losses in naturally fractured reservoirs: the effect of rheology. SPE Drill. Complet. 25 (4), 509–517.

Morris, J.P., Chochua, G.G., Bogdan, A.V., 2015. An efficient non-Newtonian fluid-flow simulator for variable aperture fractures. Can. J. Chem. Eng. 93 (11), 1902–1915.

Onyia, E.C., 1994. Experimental data analysis of lost-circulation problems during drilling with oil-based mud. SPE Drill. Complet. 9 (1), 25–31.

Robertson, R.E., Stiff Jr., H.A., 1976. An improved mathematical model for relating shear stress to shear rate in drilling fluids and cement slurries. Soc. Petrol. Eng. J. 16 (1), 31–36.

Rodríguez de Castro, A., Radilla, G., 2017. Flow of yield stress and Carreau fluids through rough-walled rock fractures: prediction and experiments. Water Resour. Res. 53 (7), 6197–6217.

Wrobel, M., 2020. An efficient algorithm of solution for the flow of generalized Newtonian fluid in channels of simple geometries. Rheol. Acta 59 (9), 651–663.

Zimmerman, R.W., Kumar, S., Bodvarsson, G.S., 1991. Lubrication theory analysis of the permeability of rough-walled fractures. Int. J. Rock Mech. Min. Sci. Geomech. Abstracts 28 (4), 325–331.